

Large-FSR Thermally Tunable Double-Ring Filters for WDM Applications in Silicon Photonics

Volume 9, Number 1, February 2017

C. L. Manganelli, *Student Member, IEEE*

P. Pintus, *Member, IEEE*

F. Gambini, *Student Member, IEEE*

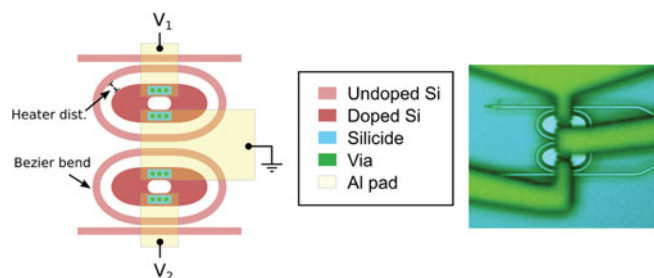
D. Fowler

M. Fournier

S. Faralli

C. Kopp

C. J. Oton



DOI: 10.1109/JPHOT.2017.2662480

1943-0655 © 2017 IEEE

Large-FSR Thermally Tunable Double-Ring Filters for WDM Applications in Silicon Photonics

C. L. Manganelli,^{1,2} *Student Member, IEEE*,
P. Pintus,^{1,2} *Member, IEEE*, F. Gambini,^{1,2} *Student Member, IEEE*,
D. Fowler,³ M. Fournier,³ S. Faralli,¹ C. Kopp,³ and C. J. Oton^{1,2}

¹Scuola Superiore Sant'Anna Pisa, Istituto Tecip, Pisa 56124, Italy

²CNIT Photonic Networks National Laboratory, Pisa 56124, Italy

³CEA LETI, Minatoc, Grenoble 38054, France

DOI:10.1109/JPHOT.2017.2662480

1943-0655 © 2017 IEEE. Translations and content mining are permitted for academic research only.

Personal use is also permitted, but republication/redistribution requires IEEE permission.

See http://www.ieee.org/publications_standards/publications/rights/index.html for more information.

Manuscript received December 7, 2016; revised January 19, 2017; accepted January 29, 2017. Date of publication February 2, 2017; date of current version February 16, 2017. This work was supported by the European Union through the Seventh Framework Programme Project IRIS under Grant 619194. Corresponding author: C. L. Manganelli (e-mail: c.manganelli@sss.up.it).

Abstract: We present the design procedure and experimental results of thermally tunable double ring resonators for integrated wavelength division multiplexing applications. A detailed analytical model specific for double rings is described, and a modified racetrack geometry using Bezier bends is used to reduce bending loss. We demonstrate devices with a free-spectral-range up to 2.4 THz (19 nm) around 1550 nm and nonadjacent channel rejection higher than 35 dB. The experimental results of thermally tunable double ring resonators is also presented with doped silicon integrated heaters, allowing the device to be used as a tunable filter or a switch.

Index Terms: Integrated optics, optical switches, ring resonators.

1. Introduction

Silicon photonic technology is highly promising for scalable integrated switch matrices due to its potential for achieving extremely small sizes and for being complementary metal–oxide semiconductor (CMOS)-compatible. Ring resonators have been widely used as filters and modulators providing very compact and efficient basic switching elements [1], [2]. However, the performance of wavelength division multiplexing (WDM) switching matrices based on a single ring add/drop filter is fundamentally limited in terms of neighbor channel rejection for a given channel bandwidth [3], [4]. In order to improve the filter performance, the strategy may be the introduction of coupled [5]–[9] or higher-order resonators [10]–[14], the exploitation of the Vernier effect [15], [16], or the investigation of transmission zero engineering [17]. The aim is to simultaneously improve the pass-band flatness, filter roll-off and channel rejection. For instance, to achieve 35 dB channel isolation, a single ring with a Q -factor of around 5000 would yield a 1-dB bandwidth of only 14 GHz (0.112 nm) and a 3-dB bandwidth of 27 GHz (0.213 nm) that may result too narrow for the signals commonly used in WDM communication systems [18]. Although several previous works have demonstrated silicon based double ring resonator filters, most of the successful demonstrations have small (around 5 nm) free-spectral ranges (FSR). The large FSR double ring resonators reported in literature present very

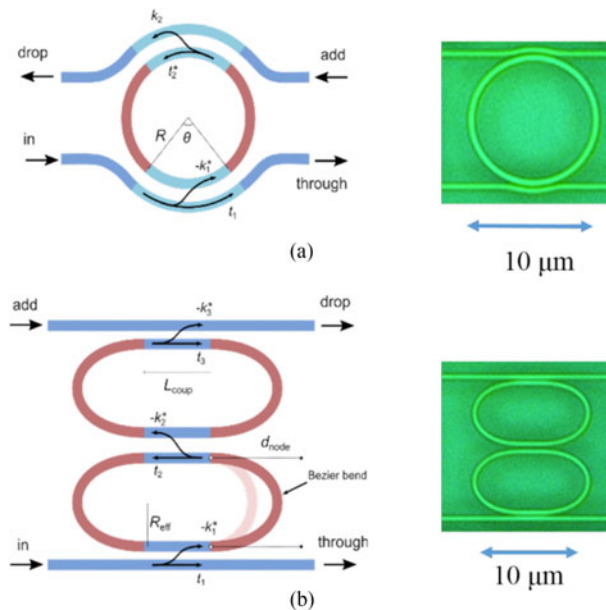


Fig. 1. Single (a) and double (b) ring schematic and relative optical microscope pictures

degrade spectra [9] or are not compatible with current standard ultra violet (UV) photolithographic processes [19]–[21] because they need less than 100 nm gap distances and they often have a limited channel rejection.

In a WDM system, the necessity of dropping only one channel from the WDM grid may require a filter with a large FSR. Since the FSR is inversely proportional to the length of the ring, very small resonators with low bend loss are required. On the other hand, the bandwidth constraint needs large coupling coefficients.

In this paper, we describe the design procedure and the successful experimental demonstration of order-two micro-ring filters, based on modified racetrack resonators obtained with Bezier bends and characterized by 2.4 THz FSR and a 3 dB bandwidth of about 100 GHz (0.8 nm). These filters are compared with single-ring filters, and show that the filtering performance of double-ring switches in terms of propagation, insertion losses and channel rejection is robust to fabrication deviations.

The last part of this paper is focused on to the characterization of integrated thermal heater fabricated with doped silicon. We report the successful tuning capabilities of these filters, and we show that small fabrication deviations, which could generate slight asymmetries in the heating, can be fully compensated by individually addressing each ring.

2. Model and Design

The add/drop ring based filters under investigation are schematically shown in Fig. 1. The single ring filter is reported in Fig. 1(a), while in Fig. 1(b), the double ring configuration is shown. In our analysis, we assume loss-less couplers, therefore the field cross-coupling coefficient and the field transmission coefficient can be expressed as $k = j\sqrt{K}$ and $t = \sqrt{1 - K}$, respectively, where K is the power coupling ratio [22]–[25]. The theory of single ring resonators is widely known in literature [1], [2]. Under the hypothesis of identical ring-waveguide couplers (i.e., $k_1 = k_2$ and $t_1 = t_2$), and negligible propagation loss, the power transmission coefficient from the input port to the drop port is

$$T_{drop} = \left| \frac{E_{drop}}{E_{in}} \right|^2 = \frac{(1 - t_1^2)^2}{1 - 2t_1^2 \cos(\beta L) + t_1^4} \quad (1)$$

where E_{in} and E_{drop} are the electric fields at the input port and at the drop port, respectively; β is the phase constant of the mode in the ring; L is the ring length; and t_1 is the field transmission coefficient

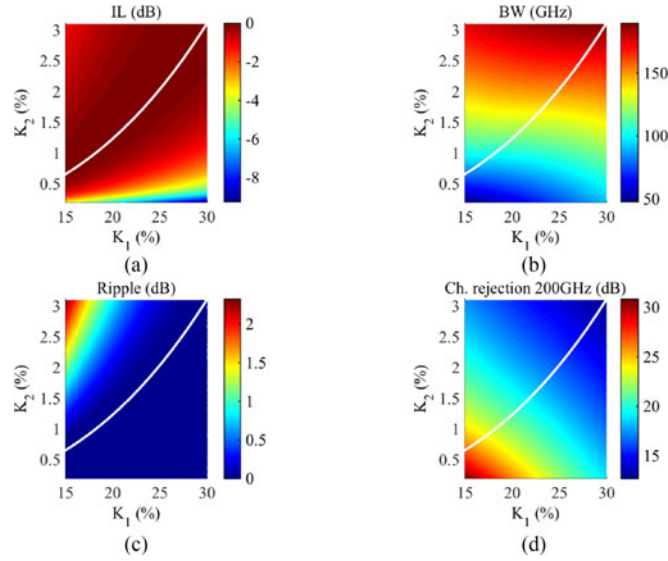


Fig. 2. Insertion loss (a), 3-dB bandwidth (b), passband ripple (c), and channel rejection (d) as functions of the bus-to-ring (K_1) and ring-to-ring coupling coefficients (K_2). The line corresponding to the impedance matching condition is shown in white.

at the ring-waveguide section. For double ring resonators, the problem can be analytically solved by using the transfer matrix method, which is reported in more detail in the Appendix. Assuming identical resonators (i.e., $L_1 = L_2 = L$ and $\beta_1 = \beta_2 = \beta$) and symmetric couplers (i.e., $k_1 = k_3$ and $t_1 = t_3$), the drop response is

$$T_{drop} = \frac{(1 - t_1^2)(1 - t_2^2)}{1 + 4t_1^2 t_2^2 + t_1^4 + 2t_1^2 \cos(2\beta L) - 4t_1 t_2 \cos(\beta L)(1 + t_1^2)} \quad (2)$$

where t_1 and t_2 are the field transmission coefficients for the bus-to-ring and ring-to-ring couplers, respectively. As we mentioned, a high-order filter shows benefits in terms of band sharpness and neighbor channel rejection. However, these filters can also show ripples which can degrade the added/dropped signal. Using the maximally-flat criterion (Butterworth-type filter) [5], we derived the impedance matching condition, i.e. when the ripples are not present. Such a condition fixes the relationship between the bus-to-ring (K_1) and the ring-to-ring (K_2) power coupling ratios

$$K_2 = \frac{K_1^2}{(2 - K_1)^2}. \quad (3)$$

The derived equation is valid also for large coupling coefficients, unlike the expressions reported in [5] that is an approximation for low K values.

Our main simulation findings for the double ring are summarized in Fig. 2. Assuming T_{drop} in (2) as a function of K_1 and K_2 , we have computed the insertion loss (IL), the 3-dB bandwidth (BW), the passband ripple, and the channel rejection for a 200 GHz (1.6 nm) spaced channel. All these parameters are defined in [25]. In the plots, the impedance matching condition is indicated with a white line. At this point, it is worth making a comparison between single and double rings in terms of the trade-off between channel rejection and bandwidth. For a FSR of 2.4 THz (~ 19 nm), we have first compared in Fig. 3 the 20-dB and 35-dB half-bandwidth Δf_{-20} and Δf_{-35} versus the 1-dB half-bandwidth Δf_{-1} for the first and second order filters, providing then an effective comparison between the two devices. From these results, the second order filter provides a significant improvement in terms of channel rejection of neighbor WDM channels when the same 1-dB bandwidth is considered.

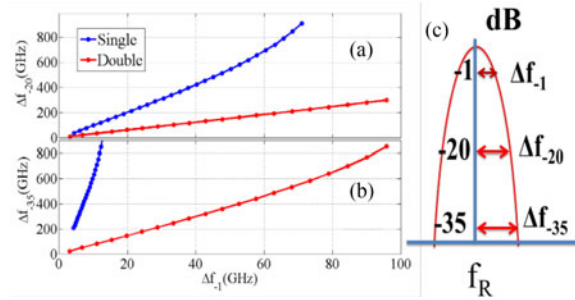


Fig. 3. Limitations of single and double rings in terms of 20 dB (a) and 35 dB (b) half bandwidth versus the 1 dB channel half-bandwidth. Definitions are shown in (c), where f_R is the resonance frequency.

3. Fabrication and Characterization

The devices were fabricated at CEA-LETI on an 8 in silicon-on-insulator (SOI) wafer with 2 μm buried oxide and 220 nm top Crystal silicon layer [26]. The silicon layer is patterned by a reactive-ion-etching (RIE) step after deep ultra-violet 193 nm optical lithography printing. Waveguides are covered with SiO_2 by chemical vapor deposition (CVD). Single polarization grating couplers with a shallow-etch depth of 70 nm are used for optical access to the input, through, and drop ports of the filter. Grating coupling loss is ~ 5 dB at $\lambda = 1550$ nm from a reference sample. Grating coupler 3 dB bandwidth is ~ 45 nm (5.62 THz).

As we already mentioned, the constraints of bandwidth and channel rejection for WDM switching matrices lead us to consider second order filters. In order to reach a maximum channel isolation of 35 dB and a 200-GHz channel rejection of 20 dB, we have designed a double ring resonator with a bus-to-ring coupling coefficient $K_1 = 20\%$ and a ring-to-ring coupling coefficient $K_2 = 1.23\%$ that is estimated from (3). Considering a circular shape and a fully-etched waveguide (to reduce the bending loss), it is difficult to reach large coupling values of 20% with a gap as small as 200 nm, even using curved couplers [21], [22]. For this reason, a racetrack-geometry is better suited, as the coupler is symmetric and can be extended. Despite this, a high FSR of 2.4 THz limits the perimeter to about 30 μm , which means bend radius smaller than 4 μm . In this case, using circular bends would yield too high loss in the transition between the straight and curved sections. For this reason, we designed bends with gradual curvature variation using Bezier-type bends, which have been used in the past to reduce bend loss in silicon photonic circuits [27]–[29]. In our case, we have used full cubic-splines 180° bends, which can be calculated using Casteljau algorithm [30] and four node positions by using the following:

$$\mathbf{R}(\zeta) = (1 - \zeta)^3 \mathbf{P}_0 + 3(1 - \zeta)^2 \zeta \mathbf{P}_1 + 3(1 - \zeta) \zeta^2 \mathbf{P}_2 + \zeta^3 \mathbf{P}_3 \quad (4)$$

where P_i for $i = 1, 2, 3, 4$ are the node positions; ζ is a dimensionless parameters which varies between 0 and 1; and \mathbf{R} is the bend trajectory. The node positions \mathbf{P}_0 and \mathbf{P}_3 are the initial and final points of the bend (the white squares in Fig. 1(b)), while \mathbf{P}_1 and \mathbf{P}_2 (represented with black squares in the same figure) determine the sharpness of the bend. We define the node distance d_{node} as the distance between \mathbf{P}_0 and \mathbf{P}_1 , which is the same as between \mathbf{P}_3 and \mathbf{P}_2 . If we normalize that number with the effective radius, we obtain a dimensionless parameter which we call normalized node distance $\delta_{node} = d_{node}/R_{eff}$. This parameter is used to identify the shape of the bend, considering that $\delta_{node} = 1.3$ corresponds to a bend which resembles a circular bend whose curvature radius is of 3 μm in terms of footprint. In order to evaluate the performance of the Bezier bends, a very high number of them have been fabricated (up to 480 bends in series), set at random distances to suppress periodic interference. The waveguide cross section was 220 nm \times 480 nm. Fig. 4 shows the total loss per bend, including transition loss, bend loss due to radiation, and loss due to unavoidable sidewall roughness.

An improvement by a factor 3 was measured for the loss between the circular and Bezier bends, for the 3 values of δ_{node} parameter under investigation (1.7, 2.0, and 2.4). It is worth noting that

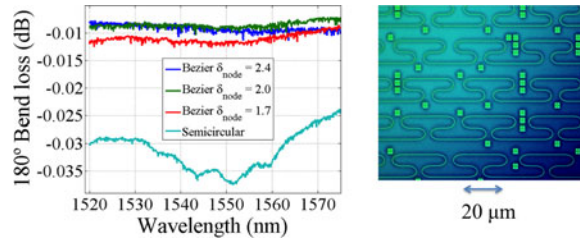


Fig. 4. 180° bend loss spectra for different normalized node distances δ_{node} fixing $R_{eff} = 3 \mu\text{m}$ and for semicircular bend and relative optical microscope pictures.

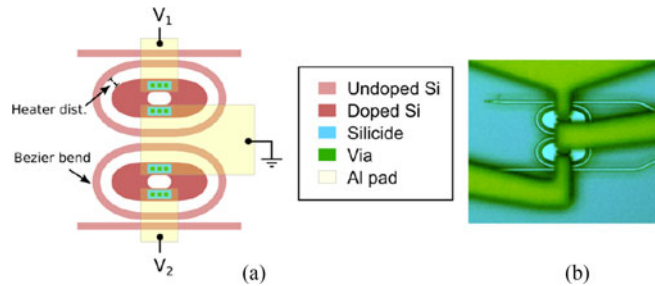


Fig. 5. Coupled ring sections with doped silicon heating element (a) and relative optical microscope picture (b).

the mode in a standard waveguide cross section ($220 \text{ nm} \times 480 \text{ nm}$) is strongly confined, so high coupling coefficients require long coupling lengths. To reach a power coupling ratio of 20% with a short coupling length, the width was decreased. For this purpose, two waveguide widths have been considered: 450 nm and 410 nm. Therefore the coupling length of the couplers is fixed to $2.2 \mu\text{m}$ and the gap distances were calculated for the two different waveguide widths. For a 410 nm wide waveguide, the gaps $g_1 = 208 \text{ nm}$ and $g_2 = 386 \text{ nm}$ are considered for ring-to-waveguide and ring-to-ring coupler, respectively; while 450 nm-wide waveguides had $g_1 = 158 \text{ nm}$ and $g_2 = 320 \text{ nm}$, respectively.

On all of these passive structures, p-type doped silicon heaters are designed and manufactured, as shown in Fig. 5. The p-doped concentration was 10^{19} cm^{-3} , which generated a sheet resistance of $480 \Omega/\text{sq}$ on 220 nm-thick silicon slab. Silicide is used to improve electrical contacts between vias and silicon slab. Our main analysis in terms of heating efficiency will be focused on the role played by the distance between the heaters, centered in the inner area of the rings, and the ring waveguide. The selected values for this distance are $0.5 \mu\text{m}$, $0.75 \mu\text{m}$ and $0.92 \mu\text{m}$.

3.1 Passive Characterization

Fig. 6(a) shows spectra of double rings drawn with the three different values of δ_{node} . Fig. 6(b) shows the transmission spectra for four instances of double rings within the same chip. Two devices are characterized by a waveguide width of 410 nm and two of them are 450 nm wide for $\delta_{node} = 2.0$. The spectral responses of the drop ports are normalized with the response of the grating couplers. This was obtained from the out-of-resonance data of the through port of each individual device, and interpolation of the on-resonance narrow regions; this was done in order to get the most accurate normalization curve as possible for each filter. For each waveguide width, the spectra of the two replicas overlap, showing a good repeatability. If fabrication inaccuracy makes the rings non-identical, the first symptom is an increased loss in the drop transmission, which was not observed in any of the spectra shown in Fig. 6.

Fig. 7 shows a comparison between single and double rings. The double ring corresponds to the case of 410 nm width, $K_1 = 20\%$ and $K_2 = 1.23\%$, while the single ring corresponds to

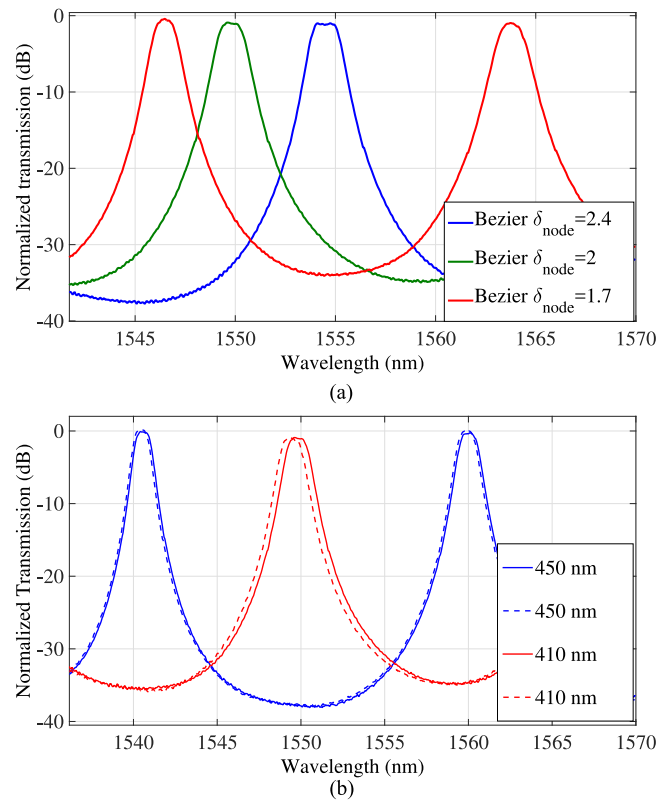


Fig. 6. Measured double ring spectra for different geometries of the Bezier bends with waveguide width of 410 nm (a). Measured double ring spectra for the different values of the waveguide width (b).

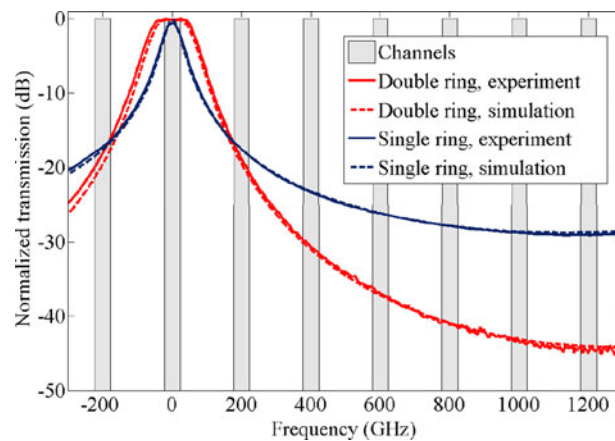


Fig. 7. Drop-port transfer function of single (blue) and double micro-rings (red). Solid lines represent the experiments, and dashed lines, the simulations. Zero frequency corresponds to ~ 1555 nm wavelength.

480 nm-wide cross section and $K = 7\%$. Simulations, which are also included in the plot, show a good agreement between theory and experiment. A 200 GHz-spaced channel grid is also shown, in order to evaluate the channel rejection of each specific channel. It is clear that both channel rejection and filter flatness are greatly improved in double rings with respect to the single ring case, leading us to conclude that second order filters represent a more suitable solution for WDM on-chip switching applications.

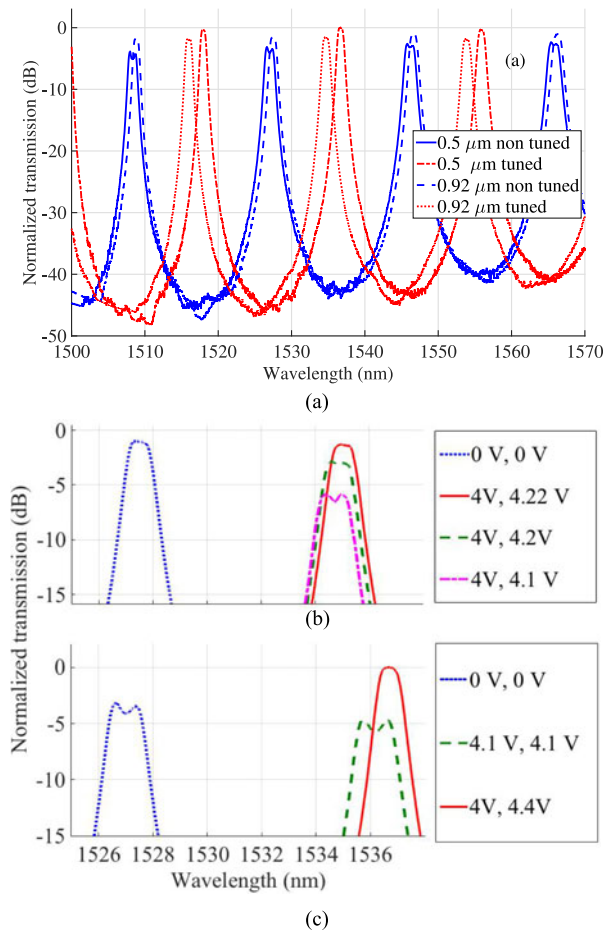


Fig. 8. Coupled ring spectra with doped silicon heaters for distances of $0.5 \mu\text{m}$ and $0.92 \mu\text{m}$ and waveguide width of 450 nm , in presence or absence of thermal tuning. (a) zoomed plot with the gradual improvement in response when the asymmetry is electrically compensated for heater distance of $0.5 \mu\text{m}$ (b) and $0.92 \mu\text{m}$ (c). In the legend of panels (b) and (c), there are the voltages applied on each ring in thermal tuning process.

3.2 Thermal Tuning

Fig. 5 shows how the heaters of each ring have a common ground but a separate voltage input. The purpose of this control arrangement is to guarantee the possibility of recovering slight asymmetries in the heating efficiency that may arise from fabrication inaccuracies. If the resonators optical paths are not identical, their resonance shift may not coincide. However the asymmetry can be compensated applying slightly different voltages to the rings. The double ring tunable filter described in [8] presents a single control voltage for both the rings at the price of lower FSR (12 nm) and finesse (hence lower sensitivity to heater asymmetry). In Fig. 8, the thermal resonance red-shift is reported for double ring resonators with 410 nm waveguide width and heater distance of $0.5 \mu\text{m}$ and $0.92 \mu\text{m}$. The measured resistances are respectively of 870Ω and 980Ω . We experimentally proved and reported more in detail in panels (b) and (c) that the filter shape asymmetry can be fully recovered with an electrical compensation of around 5% for both the heater distances. The tension applied and the power consumption in each step of the tuning activity are reported in Table 1. Different effects can contribute to the asymmetry shown in Fig. 8 including not only fabrication inaccuracy but also non identical resistance of the two different electrical paths. It is worth noting that the pads in the tested structures were not set at the same distance, having a possible influence on the spectrum degradation. Further work is in progress to assess whether independent control

TABLE 1
Applied Tension and Relative Power in Thermal Tuning Activity for different Heater Distances

Heater distance (μm)	Non tuned	Tuning 1	Tuning 2	Tuning 3
0.5	0 V, 0 V 0 mW, 0 mW	4 V, 4.22 V 18.92 mW, 20.22 mW	4 V, 4.2 V 18.88 mW, 20.08 mW	4V, 4.1 V 18.96 mW, 19.19 mW
0.92	0 V, 0 V 0 mW, 0 mW	4.1 V, 4.1 V 17.17 mW, 17.44 mW	4.1 V, 4.4 V 17.14 mW, 19.602 mW	

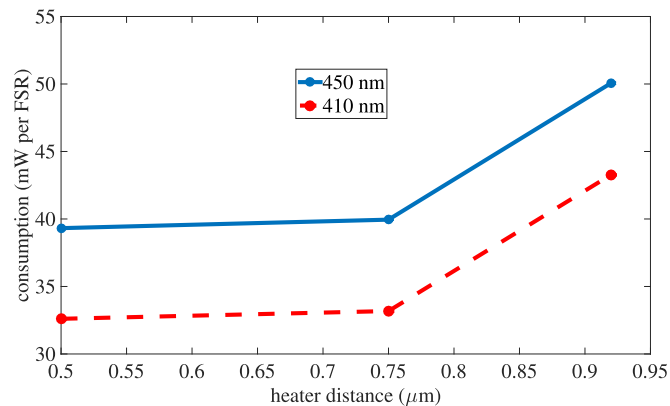


Fig. 9. Consumption per FSR and per ring as a function of the heater distance for p-type doped heater coupled rings. Different curves are for different geometries of the waveguide (450 nm and 410 nm).

is needed in a packaged device. Finally, in Fig. 9, we show the power consumption per FSR as a function of the heater distance, for waveguide widths of 450 nm and 410 nm, averaged on the two rings of each double filter. Apart from the similarities of the spectral shapes and of the curves in Fig. 8(a), the most relevant result is the expected improvement of the power efficiency for heaters closer to the waveguide. Once chosen the optimum sample at the closest distance of 0.5 μm , we calculated the average tuning consumption obtaining a value of ~ 36 mW/FSR per ring (0.69 nm/mW efficiency). This means that the total consumption of the double-ring filter is twice that value, i.e. 72 mW/FSR. We report the consumption per FSR as this number is independent on the ring perimeter, making it more easily comparable with the literature. Indeed, the consumption per FSR per ring in our experiments is lower or close too the ones reported in [8] and [9]. Special processes like local substrate removal can still improve this value of a factor of more than 10, as reported in [31].

4. Conclusion

We have shown a design procedure for a matrix switch element based on single and double ring resonators with large FSR, together with experimental results. We first introduce the analytical model and propose a modified racetrack-shaped geometry using Bezier bends. The performance of passive single and double rings are then theoretically analyzed and compared. Finally we propose an integrated heating scheme with doped silicon and we show experimental results of the tunable filter, with negligible loss when the ring asymmetry is electrically compensated.

Appendix

For double ring resonators, the problem can be solved by using a transfer-matrix method, as shown in [22]–[25]. Although the general procedure has been described in [24], here we present the explicit analytic formulation for the double-ring case. The matrix equation that links ingoing and outgoing fields in a double ring resonator is

$$\begin{pmatrix} E_{th} \\ E_{drop} \end{pmatrix} = \begin{pmatrix} t_{11} & t_{12} \\ t_{21} & t_{22} \end{pmatrix} \begin{pmatrix} E_{in} \\ E_{add} \end{pmatrix} \quad (5)$$

where E_{in} and E_{add} are the ingoing electric fields at the input and add port, respectively, while E_{th} and E_{drop} are the outgoing electric fields at the through and drop port, respectively. In this analysis, we assumed continuous wave operation, matching fields and negligible back reflections [1]. The t_{ij} elements defined in (7) have been computed combining the transfer matrix of the couplers

$$M_i = \begin{pmatrix} t_i & k_i \\ k_i^* & t_i^* \end{pmatrix} \quad (6)$$

and the round trip transmission factor of the two rings

$$\eta_i = \exp[(-\alpha_i + j\beta_i) L_i] \quad (7)$$

where L_i are the resonator perimeters, while α_i and β_i are the field attenuation and the phase constant of the circulating mode in each ring. In the more general case, we assumed that the coupler can be lossy (i.e., $d_i = \det(M_i) = (|t_i|^2 + |k_i|^2) < 1$ for $i = 1, 2, 3$). The final transfer functions are

$$t_{11} = \frac{t_1 - t_2^* \eta_1 d_1 - t_3^* \eta_2 [t_1 t_2 - \eta_1 d_1 d_2]}{\Delta} \quad (8)$$

$$t_{12} = t_{21}^* = -\frac{k_1 k_2^* k_3^* \eta_1^{1/2} \eta_2^{1/2}}{\Delta} \quad (9)$$

$$t_{11} = \frac{t_3 - t_2^* \eta_2 d_3 - t_1^* \eta_1 [t_2^* t_3 - \eta_2 d_2 d_3]}{\Delta} \quad (10)$$

where

$$\Delta = (1 - t_1^* t_2^* \eta_1) (1 - t_2^* t_3^* \eta_2) + |k_2|^2 t_1^* t_3^* \eta_1 \eta_2. \quad (11)$$

The last defined coefficient Δ plays a key role because it defines the resonance of the device. Indeed, the resonances of the first ring are described by $1 - t_1^* t_2^* \eta_1$, the resonances of the second ring are defined by $1 - t_2^* t_3^* \eta_2$, while $|k_2|^2 t_1^* t_3^* \eta_1 \eta_2$ takes into account the resonances in the loop made of the two rings (figure-eight shape loop [25]). The resonance wavelength split observable in double rings is due to the stronger influence of the figure-eight shape loop resonance over the single ring resonances. Using (10) and (11), we computed T_{drop} , which is shown in (2) in the hypothesis of negligible losses ($\alpha_i = 0$, for $i = 1, 2$), lossless coupler ($d_i = 0$, for $i = 1, 2, 3$), identical resonators, and symmetric couplers ($k_1 = k_3$).

References

- [1] W. Bogaerts *et al.*, "Silicon microring resonators," *Laser Photon. Rev.*, vol. 6, no. 1, pp. 47–73, 2012.
- [2] S. Feng, T. Lei, H. Chen, H. Cai, X. Luo, and A. W. Poon, "Silicon photonics: From a microresonator perspective," *Laser Photon. Rev.*, vol. 6, no. 2, pp. 145–177, 2012.
- [3] A. M. Prabhu, A. Tsay, Z. Han, and V. Van, "Ultracompact SOI microring add-drop filter with wide bandwidth and wide FSR," *IEEE Photon. Technol. Lett.*, vol. 21, no. 10, pp. 651–653, May 2006.
- [4] B. A. Dorin and W. N. Ye, "Two-mode division multiplexing in a silicon-on-insulator ring resonator," *Opt. Exp.*, vol. 22, no. 4, pp. 4547–4558, 2014.
- [5] B. E. Little, S. T. Chu, H. A. Haus, J. Foresi, and J.-P. Laine, "Microring resonators channel dropping filters," *J. Lightw. Technol.*, vol. 15, no. 6, pp. 998–1005, Jun. 1997.

- [6] F. Morichetti, C. Ferrari, A. Canciamilla, and A. Melloni, "The first decade of coupled resonator optical waveguides: Bringing slow light to applications," *Laser Photon. Rev.*, vol. 6, no. 1, pp. 74–96, 2012.
- [7] Y. Goebushi, C. Hisada, T. Kato, and Y. Kokubun, "Optical cross-connect circuit using hitless wavelength selective switch," *Opt. Exp.*, vol. 6, no. 2, pp. 535–548, 2008.
- [8] P. De Heyn *et al.*, "Fabrication tolerant four-channel wavelength-division-multiplexing filter based on collectively tuned Si microrings," *J. Lightw. Technol.*, vol. 31, no. 16, pp. 2785–2792, Aug. 2013.
- [9] M. S. Dahlem *et al.*, "Reconfigurable multi-channel second-order silicon microring-resonator filterbanks for on-chip WDM systems" *Opt. Exp.*, vol. 19, no. 1, pp. 306–316, 2011.
- [10] M. A. Popovic *et al.*, "Multistage high-order microring-resonator add-drop filters," *Opt. Lett.*, vol. 31, no. 17, pp. 2571–2573, 2006.
- [11] M. A. Popovic, C. Manolatu, and M. R. Watts, "Coupling-induced resonance frequency shifts in coupled dielectric multi-cavity filters," *IEEE Photon. Technol. Lett.*, vol. 14, no. 3, pp. 1208–1222, Feb. 2006.
- [12] P. DasMahapatra, C. Stabile, T. Rohit, Y. Kokubun, and K. A. Williams, "Optical crosspoint matrix using broadband resonant switches," *IEEE J. Sel. Topics Quantum Electron.*, vol. 20, no. 4, pp. 1–10, Jul./Aug. 2014.
- [13] J. D. Domnech, C. Munoz, and J. Capmany, "Transmission and group-delay characterization of coupled resonator optical waveguides apodized through the longitudinal offset technique," *Opt. Lett.*, vol. 36, no. 2, pp. 136–138, 2011.
- [14] D. Dai, "Passive silicon photonic integrated devices and circuits," *Adv. Photon. Congr.*, vol. 24, no. 11, pp. 11668–11676, 2016.
- [15] R. Boeck, N. A. F. Jaeger, N. Rouger, and L. Chrostowski, "Series-coupled silicon racetrack resonators and the Vernier effect: Theory and measurement," *Opt. Exp.*, vol. 18, no. 24, pp. 25151–25157, 2010.
- [16] A. Melloni and M. Martinelli, "Synthesis of direct-coupled-resonators bandpass filters for WDM systems," *J. Lightw. Technol.*, vol. 20, no. 2, pp. 296–303, Feb. 1997.
- [17] M. T. Wade, J. M. Shailine, J. S. Orcutt, and M. A. Popovic, "Asymmetric, pole-zero microring-resonator filters for efficient on-chip dense WDM multiplexers," in *Proc. Integr. Photon. Res. Conf.*, 2013, Paper IT5A.1.
- [18] M. Bahadori, S. Rumley, D. Nikolova, and K. Bergman, "Comprehensive design space exploration of silicon photonic interconnects," *J. Lightw. Technol.*, vol. 6, no. 1, pp. 2975–2987, 2016.
- [19] F. Xia, M. Rooks, L. Sekaric, and Y. Vlasov, "Ultra-compact high order ring resonator filters using submicron silicon photonic wires for on chip optical interconnects," *Opt. Exp.*, vol. 15, pp. 11934–11938, 2007.
- [20] Q. Li, M. Soltani, S. Yegnanarayanan, and A. Adibi, "Design and demonstration of compact, wide bandwidth coupled-resonator filters on a silicon on insulator platform," *Opt. Exp.*, vol. 16, p. 2247, 2009.
- [21] S. Xiao, M. H. Khan, H. Shen, and M. Qi, "Silicon-on-Insulator microring add-drop filters with free spectral ranges over 30 nm" *J. Lightw. Technol.*, vol. 26, no. 2, pp. 228–236, Jan. 2008.
- [22] J. Capmany and M. A. Muriel, "A new transfer matrix formalism for the analysis of fiber ring resonators: Compound coupled structures for FDMA demultiplexing," *Electron. Lett.*, vol. 36, no. 4, pp. 1904–1919, 1990.
- [23] A. Yariv, "Universal relations for coupling of optical power between microresonators and dielectric waveguides," *Electron. Lett.*, vol. 36, no. 4, pp. 321–322, 2000.
- [24] J. Capmany, P. Munoz, J. D. Domenech, and M. A. Muriel, "Apodized coupled resonator waveguides," *Opt. Exp.*, vol. 15, no. 16, pp. 10196–10206, 2007.
- [25] P. Pintus, P. Contu, N. Andriolli, A. D'Errico, F. Di Pasquale, and F. Testa, "Analysis and design of microring-based switching elements in a silicon photonic integrated transponder aggregator," *J. Lightw. Technol.*, vol. 31, no. 24, pp. 3943–3955, Dec. 2013.
- [26] J. M. Fedeli, R. Orobtcouk, C. Seassal, and L. Vivien, "Integration issues of a photonic layer on top of a CMOS circuit," *Proc. SPIE*, vol. 6125, 2006, Art. no. 61250H.
- [27] W. Bogaerts and S. K. Selvaraya, "Compact single-mode silicon hybrid rib/strip waveguide with adiabatic bends," *IEEE Photon. J.*, vol. 3, no. 3, pp. 422–432, Jun. 2011.
- [28] L. Chrostowski and M. Hochber, *Silicon Photonics Design: From Devices to System*. Cambridge, U.K.: Cambridge Univ. Press, 2015.
- [29] H. P. Bazargani, J. Flueckiger, L. Chrostowski, and J. Azana, "Microring resonator design with improved quality factors using quarter Bezier curves" in *Proc. Conf. Lasers Electro., Opt.*, 2015, pp. 1–2.
- [30] H. Phien and N. Dejdumrong, "Efficient algorithms for Bezier curves," *Comput. Aided Geom. Design*, vol. 17, no. 3, pp. 247–250, 2000.
- [31] A. Masood, M. Pantouvaki, and G. Lepage, "Comparison of heater architectures for thermal control of silicon photonic circuits" in *Proc. IEEE 10th Int. Conf. Group IV Photon.*, 2013, pp. 83–84.